Int. J. Nonlinear Anal. Appl. 15 (2024) 2, 333–358
ISSN: 2008-6822 (electronic)
http://dx.doi.org/10.22075/ijnaa.2023.30070.4324

Protection and optimization of equipment from So2 and So3

Ahmed Kamil Ghadeer[a,*], Ekbal M. Seed[b], Hayder A.H. Alguboori[b]

[a]Department of Construction and Projects, University Presidency, Thi-Qar of University, Iraq

[b]Department of Metallurgical Engineering, College of Materials Engineering, University of Babylon, Iraq

(Communicated by Ehsan Kozehgar)

Abstract

Corrosion that occurs in concentrated sulfuric acid production plants causes damage to equipment, pipes, tanks, and pumps, which affects the cost of maintenance time, which causes production stoppage and danger to workers due to the high acid concentration. The researchers used several types of alloys that help sustain production with different protection methods. Some of them are expensive, and some are highly corrosive, such as iron alloys, nickel alloys, polymers, and others in factory equipment. The current work is devoted to obtaining an alloy with mechanical and corrosive properties comparable to what is used in the concentrated sulfuric acid production plant in Iraq and the world to be used in the most important components of pipes and tanks to preserve the concentrated acid in the factory. Various alloys of a group of elements with an iron base were used and produced by the powders metallurgy method to achieve this purpose. Mechanical, corrosion tests and inspection (hardness, microstructure, dry slip corrosion, wear/abrasion, slight immersion, and Tafel testing were performed, XRD, EDX, SEM) The alloys used in this research are:

$A1(1\%Cr + 1\%Ni + 1\%Mo + 0.5\%Cu + 0.5\%Si + 0.1\%\ W + 0.1\%Ti + 1\%Mn)$

$A2(1\%Cr + 1\%Ni + 1.5\%Mo + 1.5\%Cu + 1\%Si + 0.2\%\ W + 0.2\%Ti + 1\%Mn)$

$A3(2\%Cr + 2\%Ni + 2\%Mo + 2.5\%Cu + 0.5\%Si + 0.2\%\ W + 0.2\%Ti + 2\%Mn)$

$A4(2\%Cr + 2\%Ni + 1\%Mo + 3.5\%Cu + 1\%Si + 0.2\%\ W + 0.3\%Ti + 2\%Mn)$

$A5(3\%Cr + 3.5\%Ni + 1.5\%Mo + 4\%Cu + 0.5\%Si + 0.5\%\ W + 0.5\%Ti + 3\%Mn)$

$A6(3\%Cr + 3\%Ni + 2\%Mo + 3\%Cu + 0.5\%Si + 1\%\ W + 1\%Ti + 3\%Mn)$

$A7(4\%Cr + 4\%Ni + 1\%Mo + 4\%Cu + 1\%Si + 2\%\ W + 1.5\%Ti + 2\%Mn)$

$A8(5\%Cr + 5\%Ni + 1.5\%Mo + 3\%Cu + 1\%Si + 1.5\%\ W + 2\%Ti + 3\%Mn)$

$A9(5\%Cr + 5\%Ni + 2\%Mo + 4\%Cu + 0.5\%Si + 2\%\ W + 3\%Ti + 3\%Mn)$

$A10(5\%Cr + 5\%Ni + 1.5\%Mo + 3\%Cu + 1\%Si + 3\%\ W + 2\%Ti + 2\%Mn)$

Compared to the reference samples, an increase in corrosion resistance, hardness, and wear was observed in A9 and A10 alloy. The corrosion rate (corrosion/corrosion) of the alloy improved by a factor of (40 to 99) % compared to the reference samples (carbon steel, stainless steel 304, alloy 310). / 310S / 310H), and A9, A10 compared to (ZERON, 100 alloys Sandvik SX, ZECOR, SARAMET 23 and 35, improving (13%) A9 and (0.8%) A10. In simple immersion, the primary carbon steel alloys suffered from corrosion compared to improving the alloy (A1 to A10); the improvement percentage was more than (99) %. Alloys (ZERON, ZECOR, Stainless Steel 304l), the improvement percentage in alloys only (A9, A10) from (24 to 55) %. The polarization test (Tafel) in concentrated acid on the alloy

*Corresponding author
Email addresses: Ahmedkg2004@yahoo.com (Ahmed Kamil Ghadeer), ekballseed@gmail.com (Ekbal M. Seed), drhayderalgibory@yahoo.com (Hayder A.H. ALguboori)

Received: January 2023 *Accepted:* March 2023

(A9 to A10) showed that the corrosion resistance of concentrated sulfuric acid was much better than that of carbon steel with a very high percentage. The improvement was about (99) % compared to carbon steel. Alloy A9 was the best in improving the resistance of carbon steel. Corrosion in all equipment and parts of the concentrated sulfuric acid plant (98%).

Keywords: Corrosion, Sulfuric Acid, Alloys Elements, Coating, Cathodic and Anodic Protection, Or Appropriate Design, Powder Metallurgy, Mixing, Compacting, Sintering, XRD, EDX, Tafel, Hardness, Wear
2020 MSC: 92E99

1 Introduction

Corrosion is the chemical change that happens to materials like metals, semiconductors, and insulators when they are exposed to the environment, a gaseous state, possibly wet, and an electrolyte that is either watery or not watery. The environment is the primary factor in the corrosion of metals. Practically all environments and media have corrosion to varying degrees. Some examples are moist air, pure water with salt, the weather in rural and urban areas, and the air in industrial areas. Other examples are vapor gases like Hydrogen sulfide, sulfur dioxide, chlorine, and ammonia are all gases used in fuel gas. like carbon monoxide and dioxide, and mineral acids like hydrochloric, sulfuric, and nitric acids. Organics include acetic and palmitic, different types of soil, as well as organic solvents, oils, and many foods. Corrosion is a surface phenomenon that can be affected by factors such as material size and the liquid or gas phase that makes contact [24]. Corrosion in electrolytes was separated from gas phase high-temperature corrosion by engineers and scientists (wet, hot, and dry corrosion). Both environments and experimental effects are distinct, but basic research employs similar analytic approaches to learn about the underlying mechanisms in both [26]. Corrosion is the wearing a way of a metal's surface when it is in an environment that reacts with it. On the other hand, corrosion happens when metal and its environment interact, causing the metal to slowly break down [22]. Corrosion, on the other hand, is a form of extractive metallurgy in reverse. Hematite, for example, can be heated with carbon to produce iron. Figures (1.1 and 1.2) show how iron corrodes and rusts at the end of its life cycle [14]. There is no difference between hematite and rust in terms of composition. Air and humidity, for example, are corrosive in all settings. Seawater, freshwater, distilled water, salt water, Acidic gases, steam, and other gases are found in natural, urban, marine, and industrial environments [7]. Engineers frequently use carbon steel for its high mechanical properties and lower cost than stainless steel. Carbon steel was hard to use in many different industries, like the food and drug industries, because it corroded easily.

Figure 1: Refining-corrosion cycle

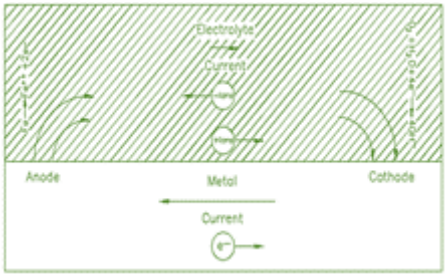

Figure 2: A diagram showing a differential corrosion cell

2 Preparation of alloys

Analysis of particle size, shape, and purity of powder

Table (1) represent purity, the particle size, source, and shape of all elements as a powder used in this study as well as source. On the other hand, table (2) shows the weight percentage of powder in each alloy.

Weight

Table 2 illustrates the following weights of the elements used in this study. The weight of each specimen was (5) g. The elements (Fe, Ni, Cr, Mo, W, Si, Ti, Mn, and Cu) as shown in table (2) [18].

Table 1: Purity, The particle size, Source, Shape of all elements

No	Element	Purity	Other				Particle Size μm	Shape	Source
1	Fe	99.99	C(0.03) % max	S(0.04) % max	P(0.02) % max		40	Irregular	India/CDH fined chemical/ Central Drug House (P) Ltd.
2	Ni	99.99					90	=	=
3	Cr	99.99					73	=	=
4	Mo	99.98					112	=	=
5	W	99.9					42	=	=
6	Si	99.96					88	=	=
7	Ti	99.98					54	=	=
8	Mn	99.89	C(0.03) % max	S(0.04)% max	P(0.02) % max	Fe (0.03) % max	102	=	=
9	Cu	99.99					111	=	=

Table 2: Weight percentage of powder in each alloy

Material / Name/ Number	Fe	Cr	Ni	Mo	Cu	Si	W	Ti	Mn	Total weight -g
A1	Bal	1	1	1	0.5	0.5	0.1	0.1	1	5
A2	Bal	1	1	1.5	1.5	1	0.2	0.2	1	=
A3	Bal	2	2	2	2.5	0.5	0.2	0.2	2	=
A4	Bal	2	2	1	3.5	1	0.2	0.3	2	=
A5	Bal	3	3.5	1.5	4	0.5	0.5	0.5	3	=
A6	Bal	3	3	2	3	0.5	1	1	3	=
A7	Bal	4	4	1	4	1	2	1.5	2	=
A8	Bal	5	5	1.5	3	1	1.5	2	3	=
A9	Bal	5	5	2	4	0.5	2	3	3	=
A10	Bal	5	5	1.5	3	1	3	2	2	=

Mixing

To guarantee uniform distribution and thorough mixing of the materials listed in table (3), mixing has been performed using a type (STGQM-1/5-2) electric rolling mixer. Because of the potential for oxidation and friction during mixing, a small amount of alcohol was utilized. Components were mixed for each alloy for equal periods (six hours) using steel balls of different sizes. The balls used in the mixing process are highly mechanical for a mixture and obtain a homogeneous distribution of the elements during mixing (as much as possible).

Table 3: Weight of all alloy powders in the mix

Elements weight in gram									
Mn	Ti	W	Si	Cu	Mo	Ni	Cr	Fe	Weight
0.25	0.03	0,03	0.13	0.25	0.25	0.38	0.25	23.70	25
0.25	0.05	0.05	0.25	0.13	0.25	0.25	0.25	23.15	25
0.50	0.05	0.05	0.13	0.38	0.38	0.50	0.50	22.15	25
0.50	0.08	0.05	0.13	0.63	0.50	0.50	0.50	22.00	25
0.75	0.13	0.13	0.13	1.00	0.25	0.88	0.75	20.88	25
0.75	0.25	0.25	0.25	0,75	0,38	0.75	0.75	20.88	25
0.50	0.38	0.50	0.25	1.00	0.50	1.00	1.00	20.13	25
0.75	0.50	0.38	0.88	0,75	0.25	1.25	1.25	19.50	25
0.75	0.75	0.50	0.25	1.00	0.38	1.25	1.25	18.88	25
0.50	0.50	0.75	0.13	0.75	0.50	1.25	1.25	19.38	25

Compacting

As shown in figure (3), compacting was done using a steel mold with a diameter of 13 mm and a height of 120 mm. After compacting, the mixed powder is pressed into green samples that are 5 mm thick and 13 mm in diameter, as shown in figure 4. Several experiments were conducted to reach the appropriate pressure starting from (400 to 750) MPa. The appropriate pressure after the experiments is (750) MPa, and the green density is (7.2) g/cm^3. Figure 5 illustrates the relationship between loads and density.

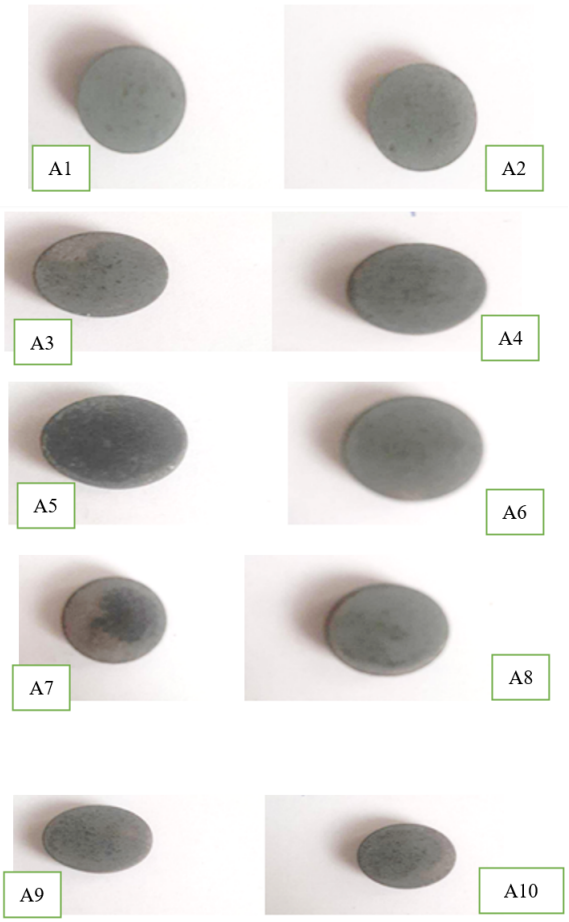

Figure 3: Samples after Compacting

Table 4: Experiments with proper pressure test

No	P (Mpa)	T (mm)	D (mm)	Area $mm^2(r^2 * \pi)$	Volume (cm^3)	density (g/cm^3)
1	400	6.0	13.0	132.7	0.8	6.3
2	500	5.9	13.0	132.7	0.8	6.4
3	550	5.7	13.0	132.7	0.8	6.6
4	600	5.6	13.0	132.7	0.7	6.7
5	650	5.4	13.0	132.7	0.7	7.0
6	700	5.2	13.0	132.7	0.7	7.2
7	750	5.2	13.0	132.7	0.7	7.2

Sintering

The sintering was carried out in an AZAR-type device made in Iran (TF 5/25 - 1500). The heat treatment was carried out as follows [4, 27, 15]:

1. Heating in a vacuum furnace at a rate of 20 °C per minute at a temperature of 1200 °C.
2. Maintain that temperature for 3 hours, then cool the samples with water at room temperature.
3. The tempering process of samples was carried out at a temperature of 250 °C using an inert gas (Argon) for 2 hours, then slow cooling inside the furnace to room temperature, as shown in figures (3.6) and (3.7).

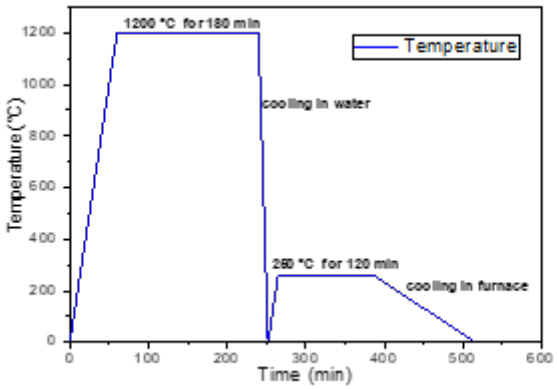

Figure 4: Sintering of all samples

Figure 5: Samples after sintering

3 Results & Discussion

Introduction

This chapter deals with the section of experimental results that have been previously obtained during practical work for all specimens. It discusses these results in different relations and evaluation of results corrosion behavior using specimen immersion test, erosion-corrosion in the factory, polarization curves, and calculate the corrosion rate at room temperature, microstructure examination, mechanical properties tests involving (hardness and wear tests). Scanning electron microscopy (SEM), XRD, and EDS are imaging topography of the specimen's surfaces.

Substrate metal test results (carbon steel)

Using an optical microscope on the substrate, figure (6) shows the microstructure of (pearlite) (Ferrite) (carbon steel) and 0.45 C medium carbon steel is widely used for shafts and gears in manufacturing, as well as some of the primary force components and steel structures. It isn't very durable or resistant to corrosion, though. Limitations to its usefulness result from its inability to satisfy practical requirements, such as abrasion and corrosion resistance. Table 5 shows how much of each element is in the steel used as a substrate; the steel sample's microstructure comprises about the same amount of ferrite and pearlite. We expect this from medium carbon steel with a higher than 0.4% carbon percentage. Figures (7) show that the analysis by (EDS) confirms that the substrate is made of carbon steel.

Table 5: The elements in steel (substrate)

C%	Si%	Mn%	S%	Cr%	M_0%	Ni%	Fe%
0.433	0.357	0.758	0.018	0.057	0.01	0.065	Bal

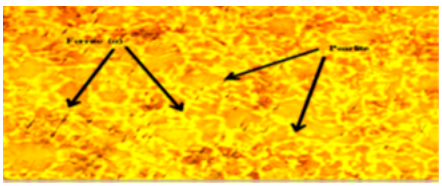

Figure 6: The carbon steel microstructure (substrate)

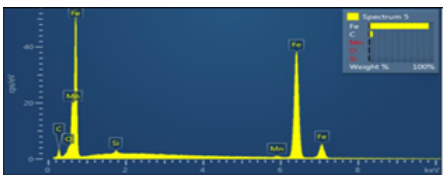

Figure 7: Substrate EDS analysis (carbon steel)

Chemical Composition

Studying and reviewing the essential alloys used in factories producing concentrated sulfuric acid to resist corrosion, such as the equipment and pipes, The chemical composition of the study shows in a table (5). Table (6) shows the chemical composition of alloys used in this study, with each element's addition of wt.% (Cr, Ni, Cu, Mo, Ti, W, Mn, Si) with the iron. this result is in agreement with those given in chapter Two (the effect of alloying elements).

Table 6: Chemical composition

Material / Namel Number	Fe	Cr	Ni	Mo	Cu	Si	W	Tl	Mn
A1	Bal	1	1	1	0.5	0.5	0.1	0.1	1
A2	Bal	1	1	1.5	1.5	1	0.2	0.2	1
A3	Bal	2	2	2	2.5	0.5	0.2	0.2	2
A4	Bal	2	2	1	3.5	1	0.2	0.3	2
A5	Bal	3	3.5	1.5	4	0.5	0.5	0.5	3
A6	Bal	3	3	2	3	0.5	1	1	3
A7	Bal	4	4	1	4	1	2	1.5	2
A8	Bal	5	5	1.5	3	1	1.5	2	3
A9	Bal	5	5	2	4	0.5	2	3	3
A10	Bal	5	5	1.5	3	1	3	2	2

X-Ray Diffraction Analysis

Figures (4.3 to 4.12) show the results of XRD analysis for all specimens. The element chromium increases where it appears in the alloys (A7 to A10). In contrast, the rest of the alloys do not appear because of their low percentage in the alloys.

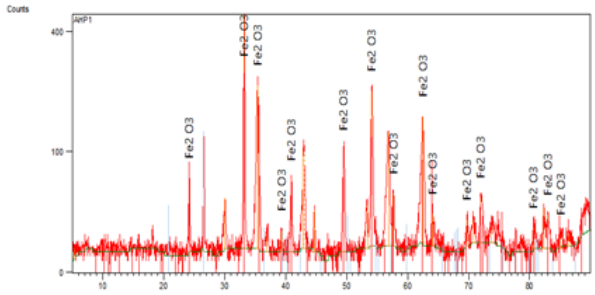

Figure 8: Xrd A1

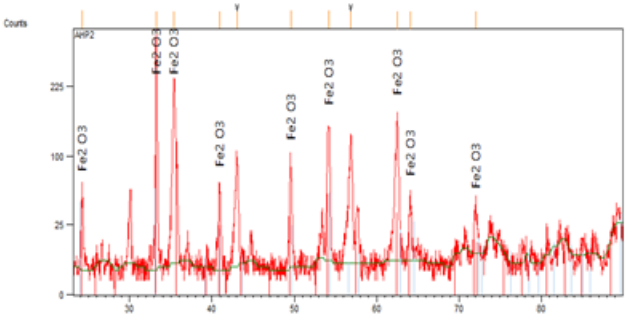

Figure 9: Xrd A2

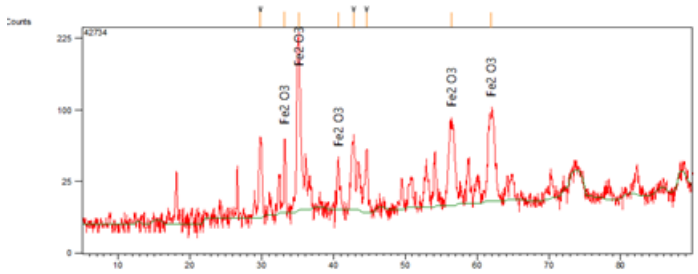

Figure 10: Xrd A3

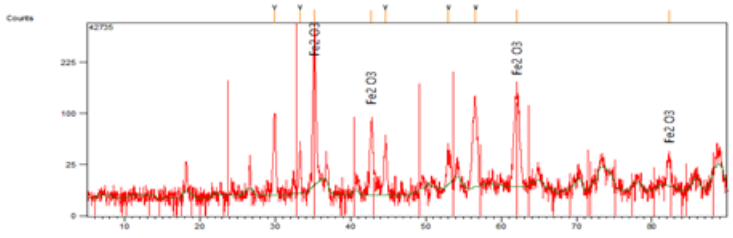

Figure 11: Xrd A4

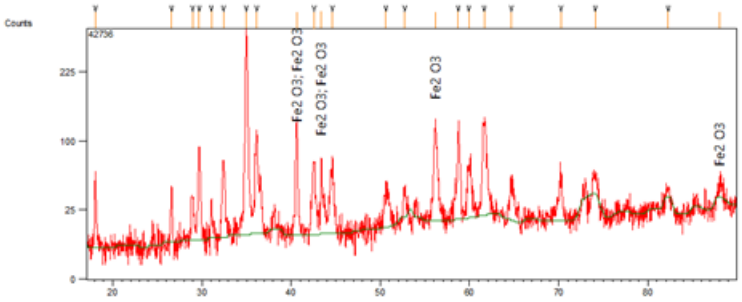

Figure 12: Xrd A5

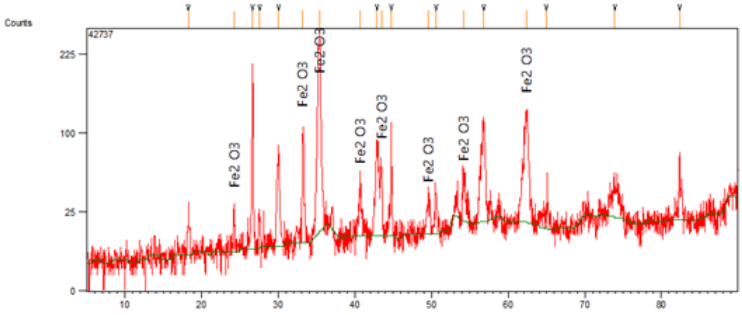

Figure 13: Xrd A6

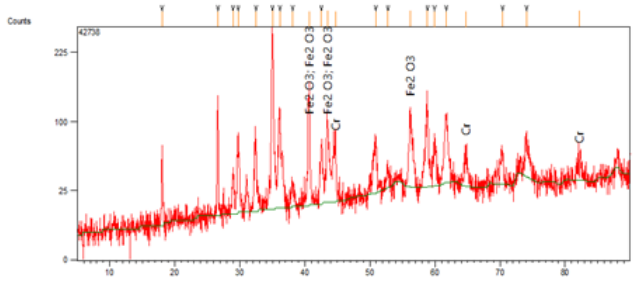

Figure 14: Xrd A7

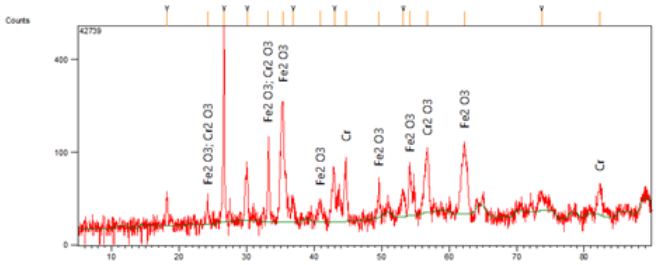

Figure 15: Xrd A8

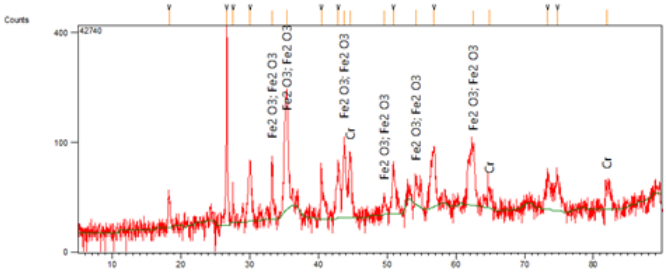

Figure 16: Xrd A9

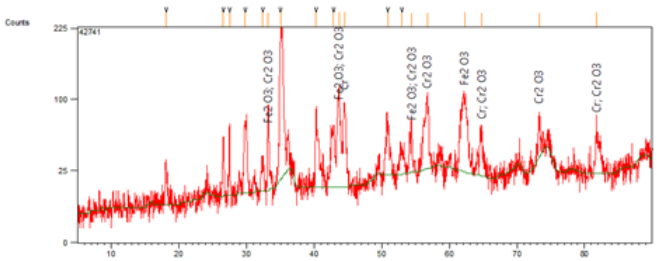

Figure 17: Xrd A10

Particle size

The size of the particles of the powder elements, as shown in table (17), and their distribution significantly affect the processing behavior of metal powders, affecting the final characteristics of powdered metals. [29]. From characteristics important, the effect size of the particles on the apparent density (inter-particle void volume and internal pore volume) materially reduces as the particle size decreases. Powder with a higher specific surface area has fewer particles [17]. As a result, the apparent density falls as the friction between particles rises. Dispersion of Particles It can increase

a powder's apparent density by inserting smaller particles between larger ones. A complicated relationship exists between compressibility and compatibility due to many variables [28]. Specifically, particle size and shape significantly impact compressibility and compatibility (also known as "green strength") [25]. When it comes to particle shape, for example, the compressibility of an irregularly shaped powder mix is lower than that of a spherical powder mix. Thus, the compressibility of spherical particles is higher than that of irregular ones. When it comes to green strength, on the other hand, particle surface area is typically enhanced [21]; because of this, the mechanical and corrosion properties improve. In all cases, fine particles are needed to optimize the part properties (density, surface quality, and mechanical properties). On the other hand, the number of big particles stays limited with the right thickness of the powder layer. Most of the time, fine particles can be melted quickly and are good for high densities, good mechanical properties, and a good scan surface. Because of this, you can expect high mechanical strength. On the other hand, larger particles help with higher breaking elongations. In alloy A9, which has elements of different grain sizes with their percentage in each alloy, it gave an excellent combination to reduce the porosity between atoms after heat treatment that improves the mechanical and corrosive properties.

Table 7: Particle size of the element

percent element in an alloy	Particle Size (μm)	Element
Bal	40	Fe
1 -5 %	90	Ni
1-5%	73	Cr
1-2%	112	Mo
0.1 - 3%	42	W
0.5 -1%	88	Si
0.1 - 3 %	54	Ti
1 -3%	102	Mn
0.5 - 4%	111	Cu

Microstructure of alloys

The previous heat treatment sample (A1) shows that the expected structure is marten site with residual austenite (γ) through rapid cooling. For tempering, the microstructure is ferrite (α) and cementite at the grain boundary. Even though the percentage of carbon in the sample is (0.03 %) of carbon, added alloying elements would dissolve in the ferrite matrix, which contributes to increasing the mechanical properties, as shown in figure (18).

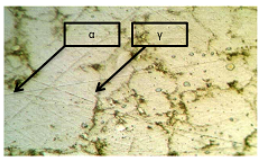

Figure 18: Microstructure of alloy A1

In the alloy (A2), in this alloy, an element (Ti, Cu, Mo, and W) has been increased, and these elements contributed to softening grains. Smoothing the grain means obtaining a smooth crystalline structure other word, the area grain boundary will increase [31, 10]; this dramatically affects mechanical and chemical properties, as shown in figure (19). There is a clear correlation between rising particle size and decreasing hardness, as seen in this graph. Grain size has a more significant impact on the visual representation of this phenomenon. For both normalized and fully annealed data, a straight line can be seen in the hardness versus space graph, as shown in figure (20). Increase in the size of grains affects corrosion - resistance, so the more significant the size of grains, the less corrosion resistance, and the opposite, as shown in Figure (21) [23].

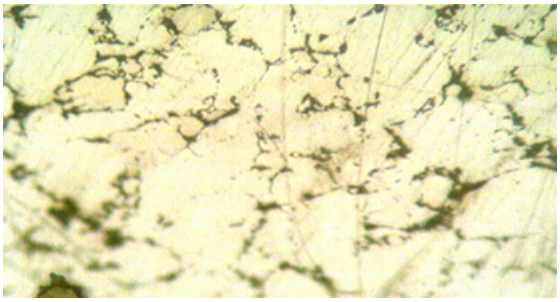

Figure 19: Microstructure of alloy A2 (X600)

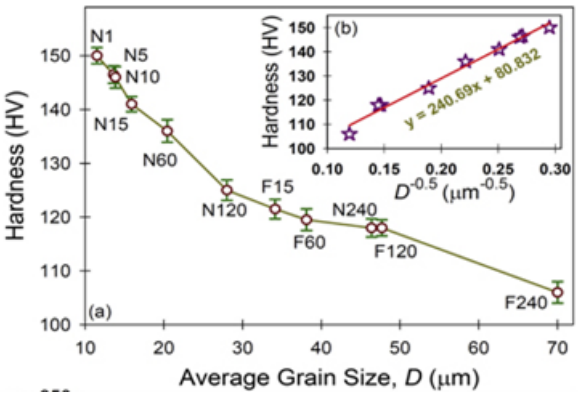

Figure 20: The relationship between particle size and hardness [23].

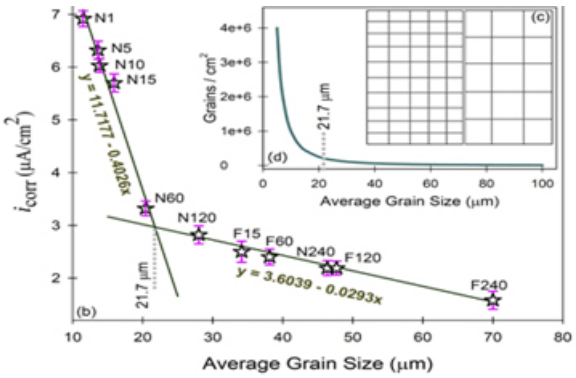

Figure 21: The relationship between particle size and corrosion

In Alloy (A3): Adding Cr encourages ferrite stability, and forming a substitutional solid solution is easy. Retained austenite was shown to be more stable with a tiny amount of (Cr) added. [13], thus improving the corrosion resistance. Nickel is one of the gamma expanders, as it improves the resistance to corrosion, oxidation, and softening of the grains. When added with Mn, it affects the microstructure and mechanical effects. When the percentage of nickel is more than 1%, it forms acicular ferrite [19]. This type of ferrite has improvement in improving the hardness of low temperatures [8]. When the (2 to 3)% ratio of nickel increases, it encourages the formation of coarse grains with grain boundaries [3].

Adding (Mo) and (Cr) to steel improves corrosion resistance, hardness resistance, and tensile strength and improves hardenability as it reduces the required cooling rate [20]. As Mo with nickel resists corrosion and resists chemical corrosion, and for this reason, it is used in the chemical industries [9]. When both (Mo, Cr, and Mn) are present, they promote the appearance of marten site or bainite structures instead of ferrite and perlite with grain boundaries because it reduces the degree of transformation of bainite [5, 6]. As for copper, in general, it increases fluidity and improves

hardness, reduces corrosion effort [1], improves steel resistance in a sulfuric environment, and crevice corrosion in acidic media [30, 2]. When the percentage of copper increases more (4%), it decreases the corrosion resistance and hardness, and the percentage is sufficient to improve the mechanical properties and corrosion [11, 12]. Manganese is one of the elements added to steel, increasing hardness and reducing critical cooling rates during hardening [16, 27]. The addition of a small percentage of Mn (2-3) % improved the plasticity of alloys and elongated the strength of the alloy by (3) %, as shown in figure (22) [15].

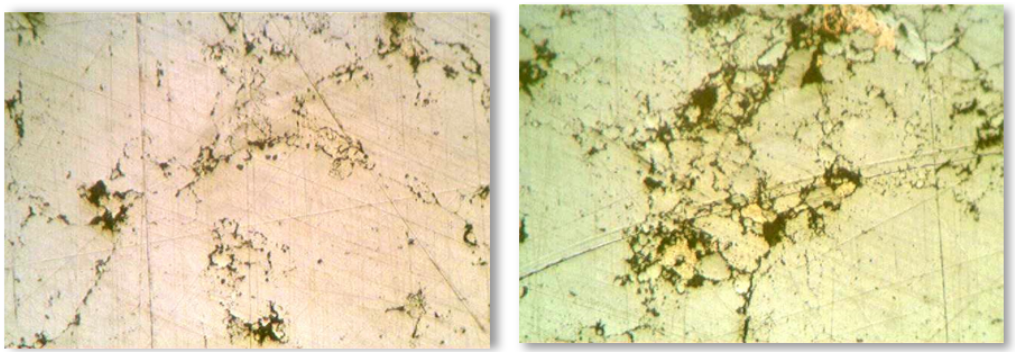

Figure 22: Microstructure of alloy A3 (X400)

When increases the proportion of copper and titanium as in alloy (A4) and other elements, increasing the rate (Ti) improves the mechanical properties and corrosion resistance; it is a stable element in steel, has a high affinity for carbon, and forms carbides, and is uniformly dispersed throughout the steel and it helps smooth the (γ and α), and the ratio of the area of the grain borders are more.

An alloy (A5, A6, A7, A8, A10) increases the proportion of (Cu, Ni, Cr). Cause the effect of these elements as in alloys (A3) elements contribute to increasing softening grains, this dramatically increasing affects mechanical and chemical properties as in figure (23). These elements also appeared in the inspection (EDX) as in figure (24).

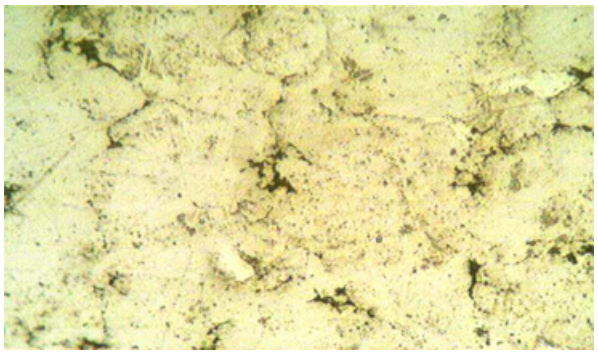

Figure 23: Microstructure of alloy A4(X600)

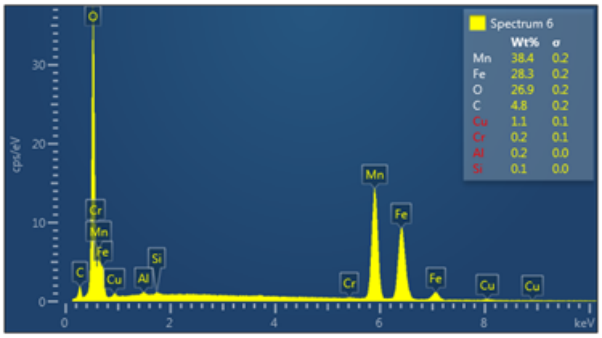

Figure 24: EDX of alloy A4

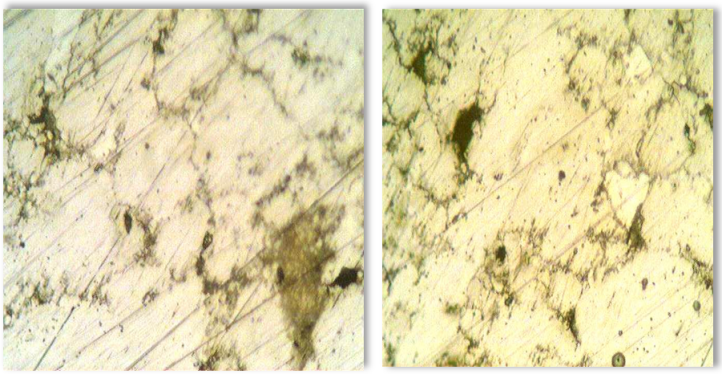

Figure 25: Microstructure of alloy A5 (X600)

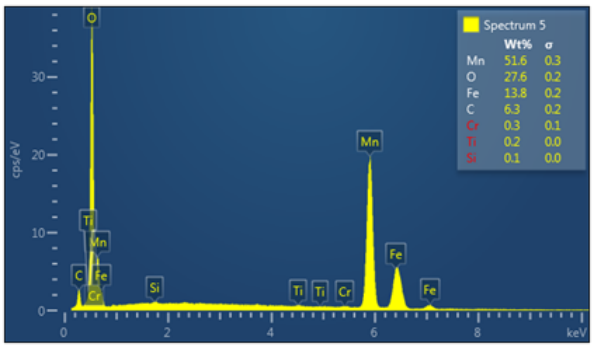

Figure 26: EDX of alloy A5

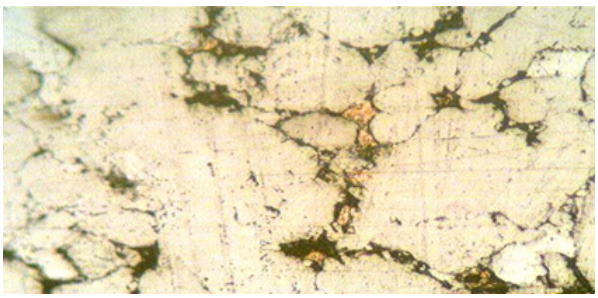

Figure 27: Microstructure of alloy A6 (X600)

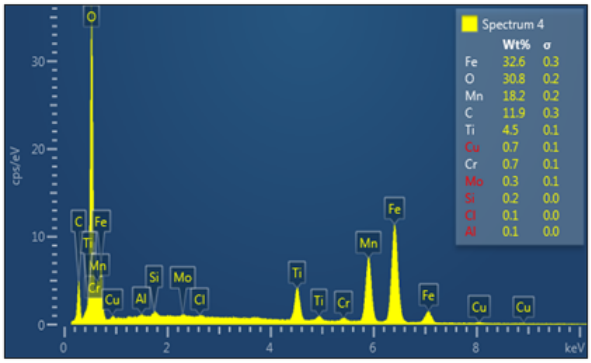

Figure 28: EDX of alloy A6

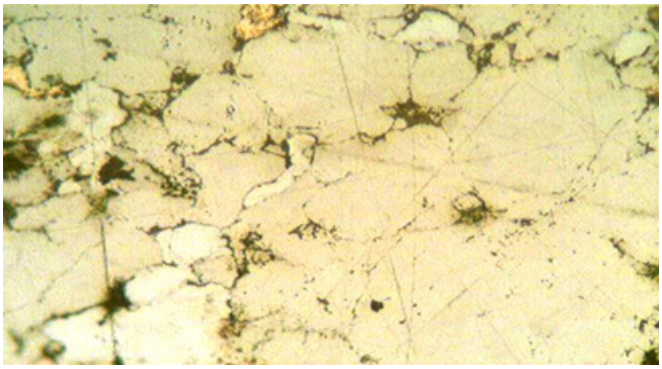

Figure 29: Microstructure of alloy A7 (X600)

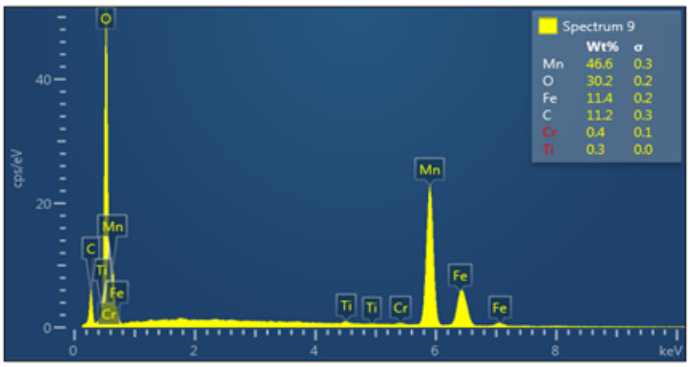

Figure 30: EDX of alloy A7

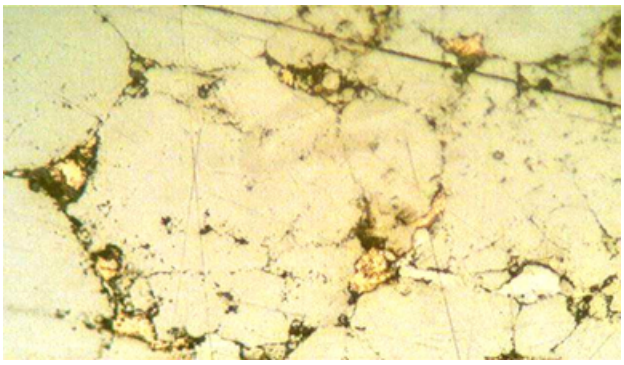

Figure 31: Microstructure of alloy A8(X600)

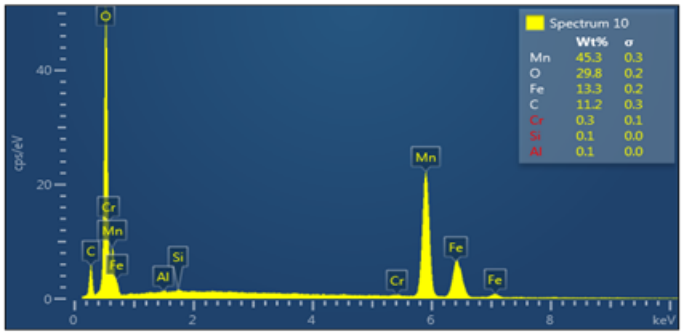

Figure 32: EDX of alloy A8

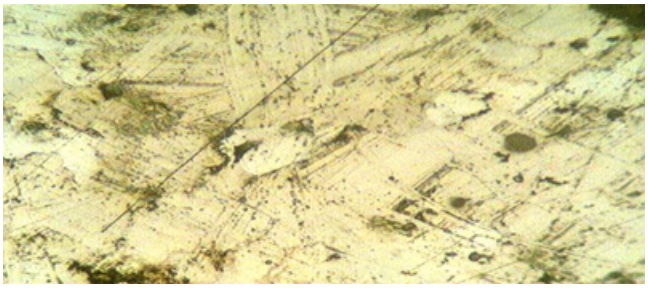

Figure 33: Microstructure of alloy A9 (X600)

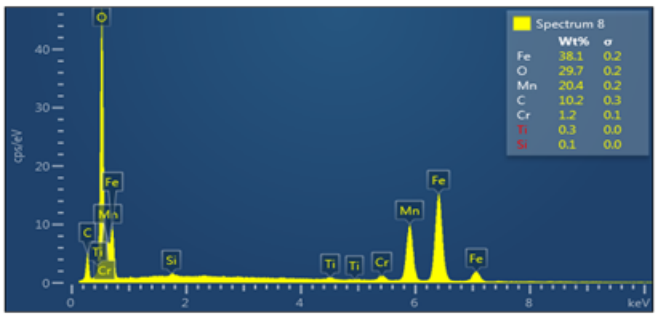

Figure 34: EDX of alloy A9

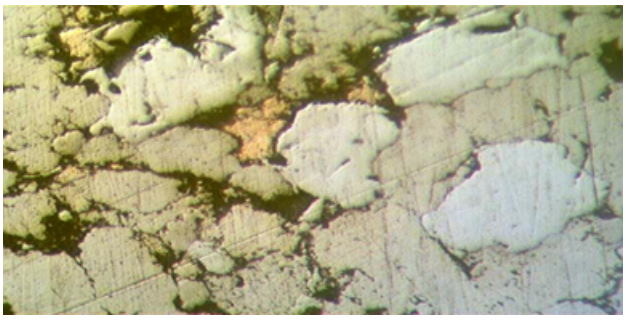

Figure 35: Microstructure of alloy A10 (X600)

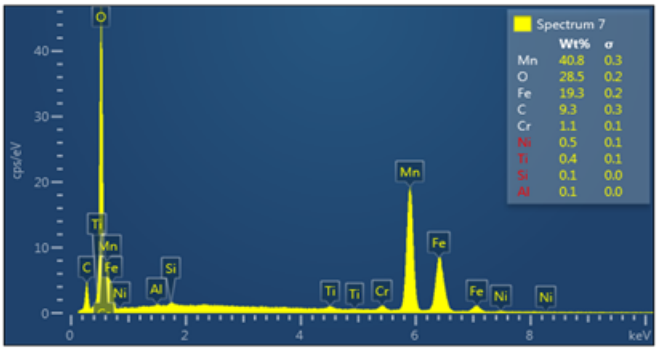

Figure 36: EDX of alloy A10

Scanning electron microscope (SEM)

Figures (4.20) to (4.27) show the results of examining the surface of the alloys with a scanning electron microscope, where we notice from the images that the alloys from (A1 to A10) resulting from the addition of elements are more

cohesive and compact with the presence of some small unincorporated masses in the ground layer of metal, because of the increased percentage of elements added to the alloy also of its deposition between the base metal.

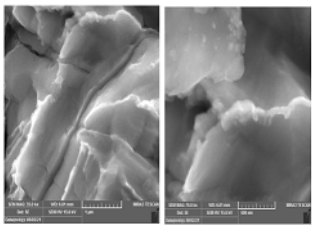

Figure 37: S.E.M (A1)

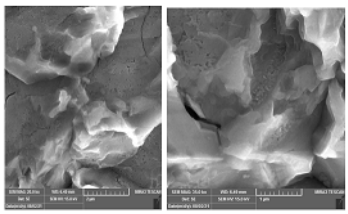

Figure 38: S.E.M (A2)

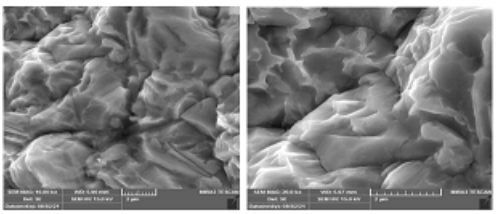

Figure 39: S.E.M (A3)

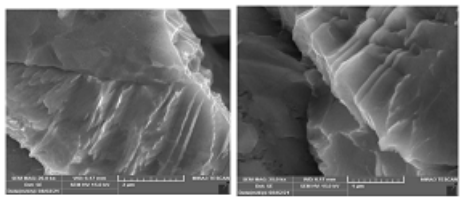

Figure 40: S.E.M (A4)

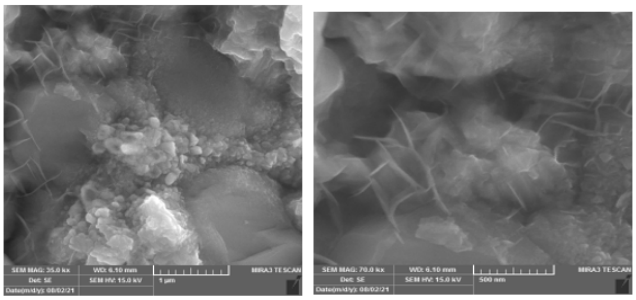

Figure 41: S.E.M (A5)

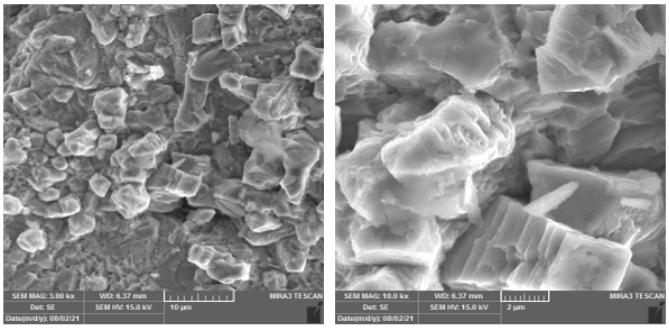

Figure 42: S.E.M (A6)

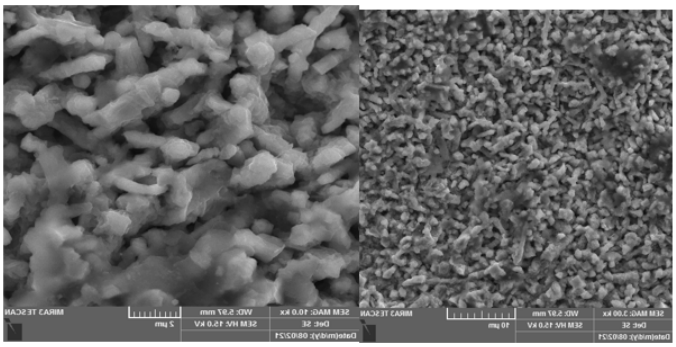

Figure 43: S.E.M (A7)

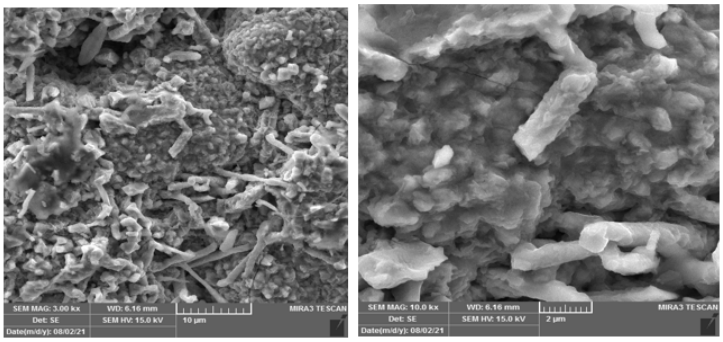

Figure 44: S.E.M (A8)

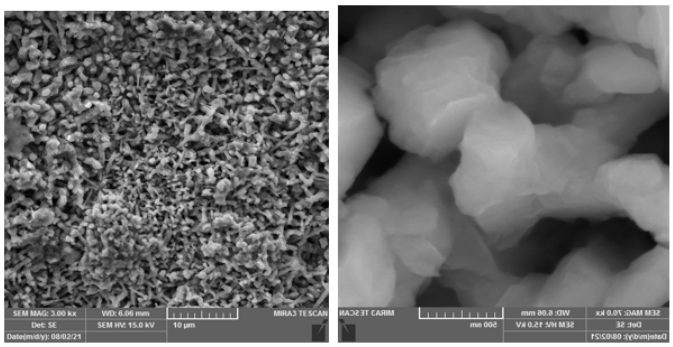

Figure 45: S.E.M (A9)

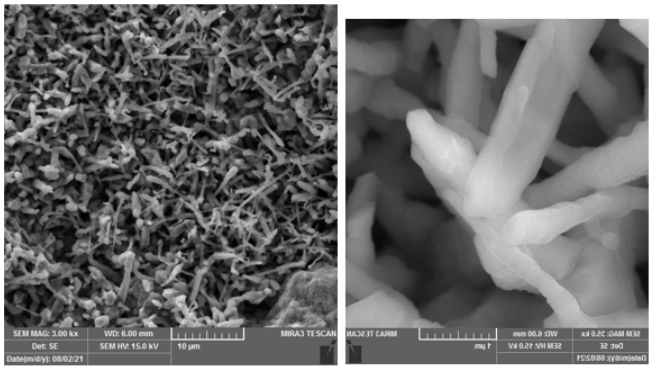

Figure 46: S.E.M (A10)

Corrosion test

Erosion /Corrosion

The corrosion test was carried out at the Al-Furat Company site. The time to complete this test was then a month. The samples were weighed weekly. The factors affecting the experiment are (sulfuric acid, acid movement speed, and acid temperature). The corrosion rate gradually decreases due to added elements that affect corrosion resistance. The alloy (A9) was more resistant to corrosion because the presence of titanium with manganese, copper, and molybdenum had an apparent effect on forming a surface layer resistant to corrosion. As well as, the deposition of some elements between the grain boundaries helped the strong bonding between the borders with low percent carbon, leading to good corrosion resistance because carbon causes inter boundary corrosion or stress corrosion crack. Table (8) shows the corrosion values between the alloys and the base metal (carbon steel).

Table 8: Corrosion values (mpy) and (mm/y) with a base metal (carbon steel)

Name	Corrosion (mpy)	Corrosion (mm/y)
Carbon steel	396.3	10
A1	9.3×10^{-2}	$253 * 10^{-3}$
A2	4.2×10^{-2}	$228 * 10^{-3}$
A3	4.1×10^{-2}	$224 * \times 10^{-3}$
A4	4×10^{-2}	$223 * 10^{-3}$
A5	3.7×10^{-2}	$130 * 10^{-3}$
A6	2.8×10^{-2}	$130 * 10^{-3}$
A7	1.4×10^{-2}	$123 * 10^{-3}$
A8	0.9×10^{-2}	$111 * 10^{-3}$
A9	$0.\ 46 \times 10^{-2}$	$86 * 10^{-3}$
A10	$0.\ 93 \times 10^{-2}$	$99 * 10^{-3}$

Where the percentage of improvement between all samples is calculated according to the equation (4.1):

$$IP\% = \frac{C.R.\,(B) - C.R.(C)}{C.R(B)}\ 100 \tag{3.1}$$

Where: IP%: The improvement percentage, C.R. (b): corrosion rate for (carbon steel as base metal or other), C.R. (c): corrosion rate of all samples.

The tables (9) show that the percentage of improvement with (carbon steel, Alloy 310/310S/310H with alloys is high, reaching more than (70 to 99%). As for the rest of the alloys, the alloys (A9, A10) are better than those used in concentrated sulfuric acid due to the elements that help resist its corrosion. Through table (9, we note that alloys from (A1 to A8) are lower than ZERON alloy because the percentage of chromium is high (26%) in the alloy and Nickle (8%), which gives an advantage. However, in the alloy (A9, A10), we notice an improvement due to elements that affect the mechanical and corrosion properties, such as (Titanium, tungsten, silicon, copper, and others), which play a role in resisting concentrated sulfuric acid. Also, alloys (A1 to A8) are low compared to (SARAMET23 & 35) alloys used in concentrated sulfuric acid concentration because of the high percentage of chromium and nickel, as well

as the high percentage of silicon (5.5) %, as the silicon dissolves in the ferrite matrix and works to strengthen the ferrite. As for (Sandvik SX, ZECOR) alloy, A1 to A8 is also lower because the alloy contains (18) % high nickel and (5) % silicon, as shown in table (9)

Table 9: Improving corrosion rate of all the samples

Material	Co Ra mm/year	IP%
carbon steel	10	
A1	$253 * 10^{-3}$	97.6
A2	$228 * 10^{-3}$	97.7
A3	$22 * *10^{-3}$	97.7
A4	$223 * 10^{-3}$	97.7
A5	$130 * 10^{-3}$	98.6
A6	$130 * 10^{-3}$	98.6
A7	$123 * 10^{-3}$	98.7
A8	$111 * 10^{-3}$	98.8
A9	$86 * 10^{-3}$	99.1
A10	$99 * 10^{-3}$	99.0

Material	Co Ra mm/year	IP%
Stainless Steel -304	0.8	
A1	$253 * 10^{-3}$	70.5
A2	$228 * 10^{-3}$	71.4
A3	$224 * 10^{-3}$	71.9
A4	$223 * 10^{-3}$	72.1
A5	$130 * 10^{-3}$	83.7
A6	$130 * 10^{-3}$	83.7
A7	$123 * 10^{-3}$	84.5
A8	$111 * 10^{-3}$	86.0
A9	$86 * 10^{-3}$	89.1
A10	$99 * 10^{-3}$	87.6

Material	Co Ra mm/year	IP 0
ZERON 100	0.1	–
A1	$253 * 10^{-3}$	–
A2	$228 * 10^{-3}$	–
A3	$224 * 10^{-3}$	–
A4	$223 * 10^{-3}$	–
A5	$130 * 10^{-3}$	–
A6	$130 * 10^{-3}$	–
A7	$123 * 10^{-3}$	–
A8	$111 * 10^{-3}$	–
A9	$86 * 10^{-3}$	13.21788
A10	$99 * 10^{-3}$	0.82043

Material	Co Ra mm/yer	IP%
ZECOR	0.1	
A1	$253 * 10^{-3}$	
A2	$228 * 10^{-3}$	
A3	$224 * 10^{-3}$	
A4	$223 * 10^{-3}$	
A5	$130 * 10^{-3}$	
A6	$130 * 10^{-3}$	
A7	$123 * 10^{-3}$	
A8	$111 * 10^{-3}$	
A9	$86 * 10^{-3}$	13.2
A10	$99 * 10^{-3}$	0.82

Material	Co Ra mm/year	PP%
Alloy 310/310 S/310H	0.4	·
A1	$253 * 10^{-3}$	41.1
A2	$228 * 10^{-3}$	42.9
A3	$224 * 10^{-3}$	44.2
A4	$223 * 10^{-3}$	44.2
A5	$130 * 10^{-3}$	67.4
A6	$130 * 10^{-3}$	67.4
A7	$123 * 10^{-3}$	69
A8	$110 * 10^{-3}$	72
A9	$86 * 10^{-3}$	78.3
A10	$99 * 10^{-3}$	75.2

Material	Co Ra mm/yer	IP%
SARAMET23 & 35	0.1	
A1	0.235551	
A2	0.228113	
A3	0.224394	
A4	0.223154	
A5	0.130173	
A6	0.130173	
A7	0.123974	
A8	0.111577	
A9	0.086782	13.2
A10	0.09918	0.8

Material	Co Ra mm/yer	IP%
Sandvik SX	0.1	
A1	$253 * 10^{-3}$	
A2	$228 * 10^{-3}$	
A3	$224 * 10^{-3}$	
A4	$223 * 10^{-3}$	
A5	$130 * 10^{-3}$	
A6	$130 * 10^{-3}$	
A7	$123 * 10^{-3}$	
A8	$111 * 10^{-3}$	
A9	$86 * 10^{-3}$	13.21788
A10	$99 * 10^{-3}$	0.82043

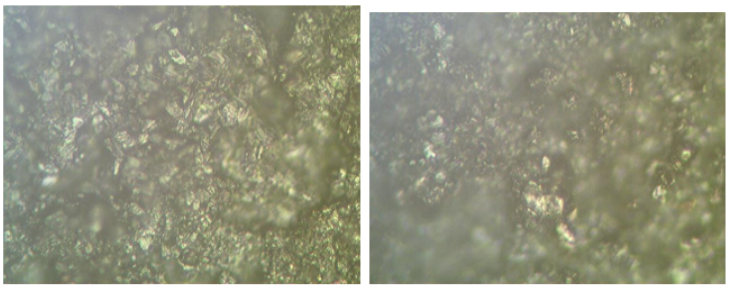

Figure 47: Microstructure Before cleaning

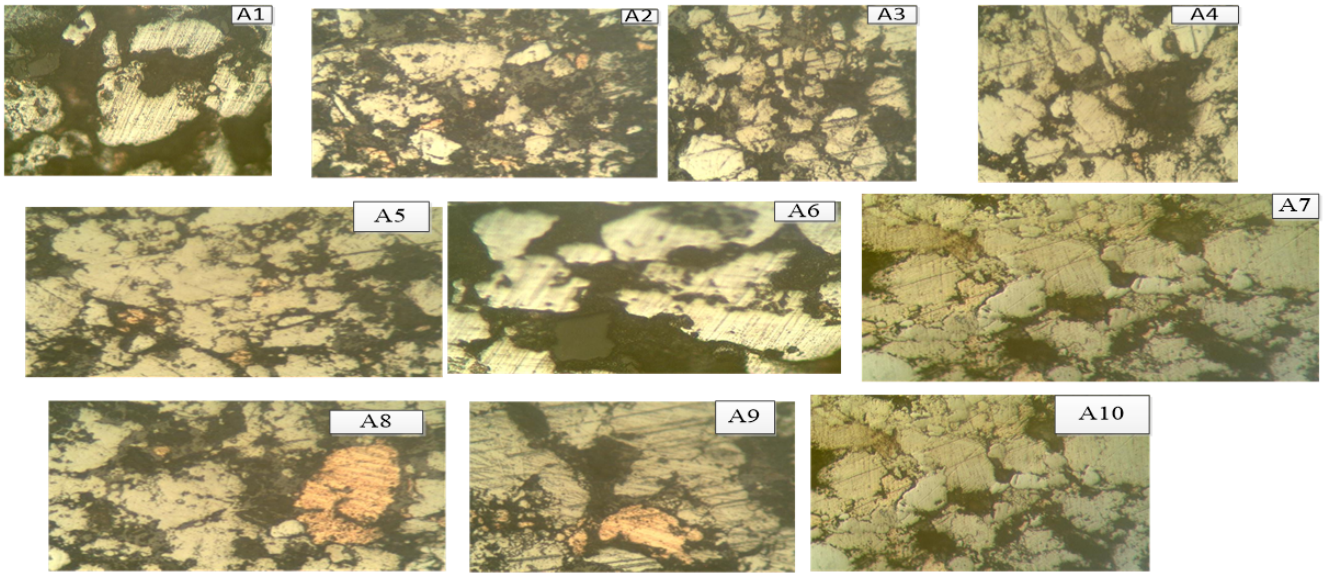

Figure 48: Microstructure after cleaning the test (Erosion)

Polarization test (Tafel)

Polarization experiments in concentrated sulfuric acid (98%) comprise voltage and current readings, where the voltage-to-logarithm current relationship is drawn. Then a (Tafel) extrapolation is made by intersecting the contact lines for both cathode and anode curves. The intersection points coordinate represent the corrosion voltage and the corrosion current by dropping.

Table 10: Polarization test factors and Corrosion rates for the models

Samples	Current density (μA/cm2)	Corrosion rate mm/y	IP%
Carbon steel	1249	10	
A1	4.251	$33.1*10^{-3}$	99.66
A2	4.169	$30.9*10^{-3}$	99.69
A3	4.132	$29.2*10^{-3}$	99.70
A4	4.044	$27.8*10^{-3}$	99.72
A5	3.92	$24.5*10^{-3}$	99.75
A6	3.499	$21.3*10^{-3}$	99.78
A7	3.21	$17.5*10^{-3}$	99.82
A8	3.204	$17.5*10^{-3}$	99.82
A9	3.0	$14.9*10^{-3}$	99.85
A10	3.2	$17.4*10^{-3}$	99.82

We note the significant improvement in reducing the corrosion rate due to using elements such as (Cr, Ni, Mn, Cu, Ti, and Mo) in the alloy (A9), which is the least ($14.9 * 10^{-3}$) mm/y. This increase led to strengthening the ferrite matrix, configuring some carbides between grain boundaries caused by some added elements compared to the corrosion rate of metal (carbon steel). These elements significantly enhance the corrosion resistance in concentrated sulfuric acid because it forms a protective layer on the alloy's surface, isolate the metal from the attack of concentrated acid and prevent or limit the surface's defects.

Specimen immersion

Table (11) includes the results of the corrosion rates of specimens in the immersion test in concentrated sulfuric acid (98%), where the results depend on the weight loss of the area exposed to the acid during a time of (60) days of each sample. The amount of improvement that occurred with carbon steel is very high, but in an alloy (ZECOR, 304L, ZERON), the percentage of improvement occurred in the alloy (A9, A10) as in the Tafel test. Figure (39) represents the relationship between sample (A9) and the percentage of increase with the rest of the alloys used because sample

(A9) represents the least corrosive samples by immersion in concentrated sulfuric acid, and this increase amounts to (100%) in the alloys.

Carbon steel and other alloys in the immersion test in concentrated sulfuric acid are subjected to corrosion. However, the corrosion rate is low compared to the corrosion rate in the case of the acid flow (Erosion test), and the temperature is higher than the ambient temperature; this is due in carbon steel to the formation of a protective layer of ferrous sulfate (FeSO4) and its stability on the surface of carbon as long as the concentrated acid (98%) is stationary or moving at little speed and natural temperatures close to the temperature of the external environment [44]. As for the rest of the alloys, the presence of a high percentage of chromium, nickel, and some elements helped form a layer of protection against corrosion so that this layer could not be removed due to acid stagnation and constant temperature. In the (erosion test), acid speed and temperature caused this layer to be removed quickly, increasing the corrosion rate [3].

Table 11: Corrosion results And Improving for all samples

name	corrosion mm / y	IP%
ZECOR	$2.5 * 10^{-4}$	–
A1	$21.5 * 10^{-4}$	–
A2	$19.7 * 10^{-4}$	–
A3	$19.5 * 10^{-4}$	–
A4	$9.74 * 10^{-4}$	–
A5	$7.93 * 10^{-4}$	–
A6	$7.39 * 10^{-4}$	–
A7	$7.31 * 0^{-4}$	–
A8	$7.93 * 10^{-4}$	–
A9	$1.12 * 10^{-4}$	55.3
A10	$1.13 * 10^{-4}$	55.4

name	corrosion mm/y	IP%
ZERON 100	$2.01 * 10^{-4}$	–
A1	$21.5 * 10^{-4}$	
A2	$19.7 * 10^{-4}$	–
A3	$19.5 * 10^{-4}$	–
A4	$9.74 * 10^{-4}$	–
A5	$7.93 * 10^{-4}$	–
A6	$7.39 * 10^{-4}$	–
A7	$7.31 * 0^{-4}$	–
A8	$7.93 * 10^{-4}$	–
A9	$1.12 * 10^{-4}$	44.26
A10	$1.13 * 10^{-4}$	44.26

name	corrosion mm/y	IP%
carbon steel	0.02	
A1	$21.5 * 10^{-4}$	89.24
A2	$19.7 * 10^{-4}$	90.15
A3	$19.5 * 10^{-4}$	90.2
A4	$9.74 * 10^{-4}$	95.13
A5	$7.93 * 10^{-4}$	96.04
A6	$7.39 * 10^{-4}$	96.04
A7	$79.31 * 10^{-4}$	96.04
A8	$7.93 * 10^{-4}$	96.04
A9	$1.12 * 10^{-4}$	99.44
A10	$1.13 * 10^{-4}$	99.43

name	corrosion mm/y	IP%
Stainless Steel - Grade 304I	$1.5 * 10^{-4}$	–
A1	$21.5 * 10^{-4}$	–
A2	$19.7 * 10^{-4}$	–
A3	$19.5 * 10^{-4}$	–
A4	$9.74 * 10^{-4}$	–
A5	$7.93 * 10^{-4}$	–
A6	$7.93 * 10^{-4}$	–
A7	$7.93 * 0^{-4}$	–
A8	$7.93 * 10^{-4}$	–
A9	$1.12 * 10^{-4}$	24.49
A10	$1.13 * 10^{-4}$	24.49

Hardness test

The hardness was calculated in the current study by the Vickers hardness method. The hardness of base alloy A1 is (165 HV); sample (A1) has the lowest hardness value compared to other samples, and this is expected because the percentage of added elements is few, as the hardness increases with the increase in the rate of elements in the remaining alloys, where elements such as (titanium, molybdenum, tungsten) work with chromium and nickel to improve the hardness resistance [20]. As (A9), the hardness (244 HV) has the highest hardness due to an increase in the proportion of (molybdenum, titanium, and manganese) as shown in figure (14). As for the comparison with the alloy used in Al-Furat Company (carbon steel), the hardness value is (190), which is lower than the alloy A3 (199 HV), where the improvement value is (4.7)% due to the increase of the elements that improve the hardness, and Alloy A9

was the highest alloy Its value is (244 HV), the improvement rate is (28.4)% compared to an alloy (carbon steel(.As for the rest of the alloys used in global factories for the production of sulfuric acid (ZERON, ZECOR), their hardness is more than the rest of the alloys (A1 to A10); the reason is that they contain 4% Mo and W more than 1%, Mn (2)%, and these elements improve their resistance to hardness as shown table (13).

Table 12: The hardness values of the base and experimental samples

Name	Hardness (H.V.)
A1	165
A.	182
A3	199
A4	210
A5	211
A6	218
A7	229
A8	232
A9	244
A10	238

Table 13: The values hardness of all samples

Name	Hardness (H.V.)
A1	165
A2	182
A3	199
A4	210
A5	211
A6	218
A7	229
A7	232
A9	244
A10	238
ZERON 100	261
Stainless Steel Grade304	201
Alloy 310/310S/310H	217
Alloy 316/316L	211
Sandvik SX	217
SARAMET23 & 35	190
ZECOR	270
carbon steel	190

Wear Test

This test method describes how to use a pin-on-disk apparatus in a lab to find out how materials wear when they slide. Most of the time, wear results are found by running a test for a certain amount of sliding distance, load, and speed. The effect of cumulative wear rate (m3/m) with sliding time (min.) for carbon steel and the other alloys are with under loads (10, 20, 30, and 40N) with different times (10, 20, 30, 40, 50, and 60 minutes).

All results from the test clearly show that alloying elements can improve and lower the wear rates of specimens. The following are two important aspects that can be obtained:

Firstly, Table (14) show a significant enhancement in wear rate behavior. For specimens (A1 to A10), improvement in wear rate was equal to (95 to 99) %, respectively, for the reference sample. The A9 sample has the lowest wear rate of the rest of the samples.

Secondly, sample A9 shows a more significant improvement in wear rate compared to the rest of the samples, and this is attributed to finer microstructure, so it has more hardness.

Table 14: Shows Improving in Wear Rate at (Load 10N & Speed 250rpm)

Sample	Wear rate $(cm^3/cm) \times 10^{-5}$ at steady state	Improving (%)
carbon steel	2.750	–
A1	0.133	95.2
A2	0.100	96.4
A3	0.100	96.4
A4	0.100	96.4
A5	0.100	96.4
A6	0.067	97.6
A7	0.050	98.2
A8	0.045	98.4
A9	0.027	99
A10	0.033	98.8

Table 15: Shows Improving in Wear Rate at (Load 20N & Speed 250rpm)

Sample	Wear rate $(cm^3/cm) \times 10^{5}$ at steady state	Improving (%)
carbon steel	3.67	–
A1	0.18	93.5
A2	0.13	95.2
A3	0.13	95.2
A4	0.13	95.3
A5	0.09	96.8
A6	0.08	97.1
A7	0.07	97.5
A8	0.06	97.8
A9	0.05	98.3
A10	0.06	97.8

Table 16: Shows Improving in Wear Rate at (Load 30N & Speed 250rpm)

Sample	Wear rate $(cm^3/cm) \times 10^{-5}$ at steady state	Improving (%)
carbon steel	5.50	–
A1	0.27	90.3
A2	0.20	92.7
A3	0.20	92.7
A4	0.19	92.9
A5	0.13	95.2
A6	0.12	95.6
A7	0.11	96.2
A8	0.09	96.7
A9	0.07	97.5
AHP10	0.09	96.7

Table 17: Shows Improving in Wear Rate at (Load 40N & Speed 250rpm)

Sample	Wear rate (cm3/cm) $\times 10^{-5}$ at steady state	Improving (%)
carbon steel	11	·
A1	0.53	80.6
A2	0.4	85.5
A3	0.4	85.5
A4	0.38	85.8
A5	0.26	90.3
A6	0.24	91.3
A7	0.21	92.4
A8	0.18	93.5
A9	0.14	94.9
A10	0.18	93.5

It is noticed that the wear rate of specimens was increasing with increasing loads (10, 20, 30, and 40N). In all loads, alloy A9 was better and less wear-resistant than other alloys, which caused outstanding improvement in the behavior of this alloy during the wear test because it comes from adding elements.

4 Conclusions

According to the results have been getting of the present work, the following points can be concluded:

1. Adding elements to the base iron alloy changes the microstructure Ferrite strengthening and smoothing, appearing as free particles precipitation inside the grain.
2. Adding elements improves the hardness and wear of the alloy while adding a more percentage of elements to the base alloy improves the hardness and wear compared to the reference specimens. The sample A9 had the highest rate of hardness and wear.
3. XRD analysis test for alloy (A1, A2, A3, A4, A5, A6) appears FeO3 phase because the content of the element in alloy doesn't exceed 4%, based on the equivalent value alloying elements such as Cr, Ni have a similar effect on the type of phases in the microstructure of the Steel. Alloys (A7, A8, and A9) appear to have elements Cr and Cr2O3 due more to than Cr 5%.
4. The addition of elements reduces the corrosion rate (Erosion /Corrosion) of alloys, improving by a factor (40 to 99) % compared to reference specimens (carbon steel, Stainless Steel 304, Alloy 310/310S/310H), and A9, A10 compared to (ZERON, 100 Sandvik SX, ZECOR, SARAMET23 & 35) alloys, improving (13%) A9 and (0.8%) A10.
5. In the simple immersion, base alloy carbon steel was mainly suffering from corrosion compared to improving an alloy (A1 to A10), and the percentage of improvement was more than (99) %. Alloys (ZERON, ZECOR, Stainless Steel 304l), the percentage of improvement in only the alloys (A9, A10) from (24 to 55) %.
6. The Polarization test (Tafel) in acid showed alloys (A9 to A10) that the corrosion resistance of concentrated sulfuric acid was much better than that of carbon steel by a very high percentage. The percentage improvement is about (99) % compared with carbon steel.
7. The alloy A9 was the best at improving the corrosion resistance in all equipment and parts of a concentrated sulfuric acid plant (98%).

References

[1] A. Abu-Oqail, M. Ghanim, M. El-Sheikh, and A. El-Nikhaily, *Effects of processing parameters of tungsten–copper composites*, Int. J. Refract. Metals Hard Mater. **35** (2012), 207–212.

[2] S. Acid, H. Acid, H. Acid, and P. Acid, *Corrosion problems and alloy solutions 1 corrosion-resistant alloys from the special metals group of companies 4 alloy selection for corrosive environments 11*, Unknown, 2000.

[3] J.B. Bacalhau and C.R.M Afonso, *Effect of Ni addition on bainite microstructure of low-carbon special bar quality steels and its influence on CCT diagrams*, J. Mater. Res. Technol. **15** (2021), 1266–1283.

[4] O. Bergman, *Key aspects of sintering powder metallurgy steel pre-alloyed with chromium and manganese*, Ph.D. thesis, Chalmers Tekniska Hogskola (Sweden), 2011.

[5] W.L. Bevilaqua, J. Epp, H. Meyer, A. Da Silva Rocha, and H. Roelofs, *In situ investigation of the bainitic transformation from deformed austenite during continuous cooling in a low carbon Mn-Si-Cr-Mo steel*, Metallurgical and Materials Transactions A **51** (2020), no. 7, 3627–3637.

[6] H.K.D.H. Bhadeshia, S.A. David, J.M. Vitek, and R.W. Reed, *Stress induced transformation to bainite in Fe–Cr–Mo–C pressure vessel steel*, Materials Sci. Technol. **7** (1991), no. 8, 686–698.

[7] Y-.S. Choi, S. Nesic, and S. Ling, *Effect of H2S on the CO2 corrosion of carbon steel in acidic solutions*, Electroch. Acta **56** (2011), no. 4, 1752–1760.

[8] A.P. Coldren and J.L. Mihelich, *Acicular ferrite HSLA steels for line pipe*, Met. Sci. Heat Treat. **19** (1977), no. 7, 559–572.

[9] P. Crook, *Corrosion characteristics of the wrought Ni-Cr-Mo alloys*, Mater. Corros. **56** (2005), no. 9, 606–610.

[10] K. Edalati and Z. Horita, *Significance of homologous temperature in softening behavior and grain size of pure metals processed by high-pressure torsion*, Mater. Sci. Eng. A **528** (2011), no. 25–26, 7514–7523.

[11] Y. Guo, Y. Zou, Y. Zheng, Y. Wang, X. Liu, Y. Wu, J. Sun, and J. Chen, *In vitro corrosion resistance and antibacterial performance of novel Fe–xCu biomedical alloys prepared by selective laser melting*, Adv. Eng. Mater. **23** (2021), no. 4, 2001000.

[12] I.T. Hong and C.H. Koo, *Antibacterial properties, corrosion resistance and mechanical properties of Cu-modified sus 304 stainless steel*, Mater. Sci. Eng. A **393** (2005), no. 1-2, 213–222.

[13] R. Hossain, F. Pahlevani, and V. Sahajwalla, *Effect of small addition of Cr on stability of retained austenite in high carbon steel*, Mater. Charact. **125** (2017), 114–122.

[14] K. Kardelen, *Investigation of pitting corrosion morphology of St 37 material in different corrosive environments*, Ph.D. thesis, Ankara Yıldırım Beyazıt University, 2018.

[15] S.-J. Lee, J. Han, S. Lee, S.-H. Kang, S.-M. Lee, and Y.-K. Lee, *Design for Fe-high Mn alloy with an improved combination of strength and ductility*, Sci. Rep. **7** (2017), no. 1, 1–9.

[16] B. Liscic, H.M. Tensi, L.C.F. Canale, and G.E. Totten, *Quenching theory and technology*, CRC Press, 2010.

[17] S. Lowell, J.E. Shields, M.A. Thomas, and M. Thommes, *Characterization of porous solids and powders: Surface area, pore size and density*, vol. 16, Springer Science & Business Media, 2006.

[18] P. Rajeev, A.O. Surendranathan, and C.S.N. Murthy, *Corrosion mitigation of the oil well steels using organic inhibitors: A review*, J. Materials Envir. Sci. **3** (2012), no. 5, 856–869.

[19] M.A. Razzak, *Heat treatment and effects of Cr and Ni in low alloy steel*, Bull. Mater. Sci. **34** (2011), no. 7, 1439–1445.

[20] R.F. Santos, A.M. Rocha, A.C. Bastos, J.P. Cardoso, F. Rodrigues, C.M. Fernandes, J. Sacramento, M.G.S. Ferreira, A.M.R. Senos, C. Fonseca, and M.F. Vieira, *Microstructural characterization and corrosion resistance of wc-ni-cr-mo composite–the effect of mo*, Int. J. Refract. Met. Hard Mater. **86** (2020), 105090.

[21] M. Shamsuddin and H.Y. Sohn, *Constitutive topics in physical chemistry of high-temperature nonferrous metallurgy: A review—part 2, Reduction and refining*, JOM **71** (2019), no. 9, 3266–3276.

[22] L.L. Shreir, *Corrosion: Metal/Environment Reactions*, Newnes, 2013.

[23] M. Soleimani, H. Mirzadeh, and C. Dehghanian, *Effect of grain size on the corrosion resistance of low carbon steel*, Mater. Res. Express **7** (2020), no. 1, 16522.

[24] C. Stampfl, M.V. Ganduglia-Pirovano, K. Reuter, and M. Scheffler, *Catalysis and corrosion: The theoretical surface-science context*, Surface Sci. **500** (2002), no. 1-3, 368–394.

[25] S.B. Sternowski, G.E. O'Donnell, and L. Looney, *Effect of particle size on the mechanical properties of sic particulate reinforced aluminum alloy AA6061*, Key Engineering Materials, vol. 127, Trans Tech Publications, 1997, pp. 455–462.

[26] H.-H. Strehblow and P. Marcus, *Fundamentals of corrosion*, Corrosion Mech. Theory Practice (2012), 1–104.

[27] G.E. Totten, C.E. Bates, and N.A. Clinton, *Handbook of Quenchants and Quenching Technology*, ASM Interna-

tional, 1993.

[28] G.S. Upadhyaya, *Powder metallurgy technology*, Cambridge International Science Publishing, 1997.

[29] S. Vock, B. Klöden, A. Kirchner, T. Weißgärber, and B. Kieback, *Powders for powder bed fusion: a review*, Prog. Add. Manufact. **4** (2019), no. 4, 383–397.

[30] B.I. Voronenko, *Austenitic-ferritic stainless steels: A state-of-the-art review*, Metal Sci. Heat Treat. **39** (1997), no. 10, 428–437.

[31] G. Voyiadjis and B. Deliktas, *Modeling of strengthening and softening in inelastic nanocrystalline materials with reference to the triple junction and grain boundaries using strain gradient plasticity*, Acta Mech. **213** (2010), no. 1, 3–26.